ISSN Print: 2347-4203 ISSN Online: 2347-4211

JOURNAL OF CIVIL ENGINEERING AND TECHNOLOGY (JCIET)

https://iaeme.com/Home/journal/JCIET

Peer Reviewed Journal

IAEME PUBLICATION

Plot: 03, Flat- S 1, Poomalai Santosh Pearls Apartment, Vaiko Salai 6th Street,
Jai Shankar Nagar, Palavakkam, Chennai - 600 041, Tamilnadu, India.

E-mail: editor@iaeme.com, iaemedu@gmail.com Website: www.iaeme.com Mobile: +91-9884798314

Journal of Civil Engineering and Technology (JCIET)
Volume 11, Issue 2, July-December 2025, pp. 1-28, Article ID: JCIET_11_02_001
Available online at https://iaeme.com/Home/issue/JCIET?Volume=11&Issue=2
ISSN Print: 2347-4203 and ISSN Online: 2347-4211; Journal ID: 3797-4210
Impact Factor (2025): 17.50 (Based on Google Scholar Citation)
DOI: https://doi.org/10.34218/JCIET_11_02_001

DEVELOPMENT OF ULTRA-LOW POWER DEICER FOR CIVIL ENGINEERING APPLICATIONS

Victor Petrenko

Thayer School of Engineering, Dartmouth College,
14 Engineering Drive, Hanover, NH 03755, United States.

ABSTRACT

Ice and snow accumulation on engineering structures, such as buildings, bridges, roads, power transmission lines, and communication and refrigeration equipment, presents serious problems. Over several decades, numerous deicing and anti-icing technologies have been invented, developed, and used. The important factors of merit of the deicing technologies are the energy and power requirements, clean removal of ice and snow from protected surfaces, safety, reliability, and cost of manufacturing and operations. The improvement of existing de- and anti-icing technologies is still in progress. We consider our research to be a valuable contribution to this field. This manuscript presents the development and design of an ultra-low-power electro-impulsive deicer for civil engineering. To drastically decrease the energy consumption of the EID, we combined the results of recent advances in low ice adhesion materials with advanced EID analytical theory and computer simulation. The result is an energy requirement 100 times less than that of the pulse electrothermal deicer (PETD) and 1000 times less than that of traditional thermal de-icing (TD). This manuscript presents simple and accurate algorithms for EID design and optimization, and the results of experimental testing of EID made of materials known for their low adhesion to ice. The

improved EID technology can be applied to the deicing of buildings, bridges, airplanes, evaporators of refrigerators, harvesting of ice in residential, commercial, and industrial icemakers, and in deicing communication equipment such as antennas and radars.

Keywords: building deicing, deicing energy, deicing power, ice adhesion, ice velocity.

Cite this Article: Victor Petrenko. (2025). Development of Ultra-Low Power Deicer for Civil Engineering Applications. *Journal of Civil Engineering and Technology (JCIET)*, 11(2), 1-28. DOI: https://doi.org/10.34218/JCIET_11_02_001

I. Introduction

Ice and snow accumulation on buildings creates numerous problems, such as structural damage, roof collapse, ice dam formation, gutter damage, exterior surface damage, roof leaks, falling icicles, safety hazards, and slip and fall accidents.

Deicing technologies are broadly categorized as active or passive systems. Active systems use energy to remove or prevent ice, whereas passive methods use building design and material properties to mitigate ice buildup. Among active deicing systems, conventional electrothermal deicers (CETD) are the most common and include:

- Heat cables and tapes.
- Heated panels and mats.
- Self-regulating technology.
- Heated liquid tubing.

The energy required to deice surfaces with CETD is approximately 1 MJ/m2 and above. More energy-efficient deicing systems include the following two technologies:

- Electro-impulsive deicing (EID) [1,2]. The EID energy requirement is typically in the range of 10 kJ/m2–20 kJ/m2, which is well below the energy required for CETD, but conventional EID systems built using aluminum sheets cannot perfectly clean protected surfaces off ice.
- Pulse Electro Thermal Deicing (PETD) [3,4]. PETD typically requires an energy density of 50 kJ/m2–150 kJ/m2. PETD quickly melts the thin ice/structure interface. However, PETD systems require an external force, such as gravity, to remove ice.

Passive de-icing systems. Passive technologies are designed to prevent ice from forming in the first place by addressing the root causes of ice dams and accumulation.

Among the active deicing systems, EID requires less energy per square meter to deice surfaces. Another advantage of EID is that it can throw ice off surfaces at a significant velocity. This is a valuable feature for building de-icing. Two known drawbacks of EID are: 1) incomplete cleaning of protected surfaces off ice, and 2) accumulation of material fatigue of protected skins (usually aluminum alloys).

EID systems are currently used in the aerospace and wind energy generation industries. Although electro-impulsive technology was used in the past for the demolition of old structures, it is not currently used for protecting buildings from ice and snow.

The objectives of our research are as follows: 1) Significant improvement of cleaning surfaces off ice. 2) Further drastic reduction in EID energy requirements. 3) Development of a simple and useful analytical theory for designing EID systems. The first and second objectives were achieved by replacing the traditional aluminum skin of EID systems with low interfacial toughness materials recommended for surface deicing [5]. To achieve the third objective, we created a combination of MathCad EID optimization software and computer simulations using COMSOL Multiphysics software.

II. EID Principles of operations and short history

To separate ice from a thin-wall structure, an EID device generates a very short (10μs to 100μs) pressure pulse and applies it to an ice/structure interface. The shock wave created by the pulse propagates along the interface and breaks the ice adhesion to the structure. EID also pushes ice and structures apart.

The use of electromagnetic impulse force to remove ice was first suggested by Rudolf Goldschmidt, a German national residing in London before World War II [6]. During the 1950s and the 1960s, electro-impulse methods were used for forming metal parts in various industrial processes, but no record can be found of the EID use for de-icing until researchers in the USSR discovered Goldschmidt's patents or rediscovered this application independently [1,2].

Since the 1970s, numerous US and foreign EID patents have been granted, and over 100 academic papers devoted to EID research have been published. Some essential examples for this study are provided in the references [7-22]. Many aerospace companies have used and are still using this technology. Some examples are COX & Company Co. (Electro-Mechanical Expulsion Deicing System (EMEDS)) and Goodrich Co. (is now a part of Raytheon Technologies). We will refer in more detail to some academic publications that relate to our research below.

The great success of EID is mainly based on its very low energy requirement of approximate range of 10kJ/m2 to 20kJ/m2 and the very low time-average power requirement of 56 W/m2–112 W/m2 at 3-min cycling. The typical power requirement for thermal anti-icing of the leading edges of airplane wings is 12 kW/m2. The known disadvantages of EID, which limit its use, are imperfect ice cleaning and fatigue of the coil and skin materials.

Most EID research publications and patents are related to aerospace applications. Civil engineering applications of EID (CEEID) differ from aerospace EID applications (ASEID) for several reasons. First, the ASEID should withstand approximately 2 million cycles, whereas the CEEID can be designed for only 2 thousand cycles. Second, while the ASEID only separates ice from an airplane skin, the CEEID throws ice off the protected structure borders.

The separation ice fragment velocity can be adjusted from zero to 20 m/s. A single wire coil (Fig. 1a), pair of wire coils (Fig. 1b), or single double-layer coil (Fig. 1c) is used to generate a pulse shock wave when a capacitor (an energy storage device) discharges through the coil or coils.

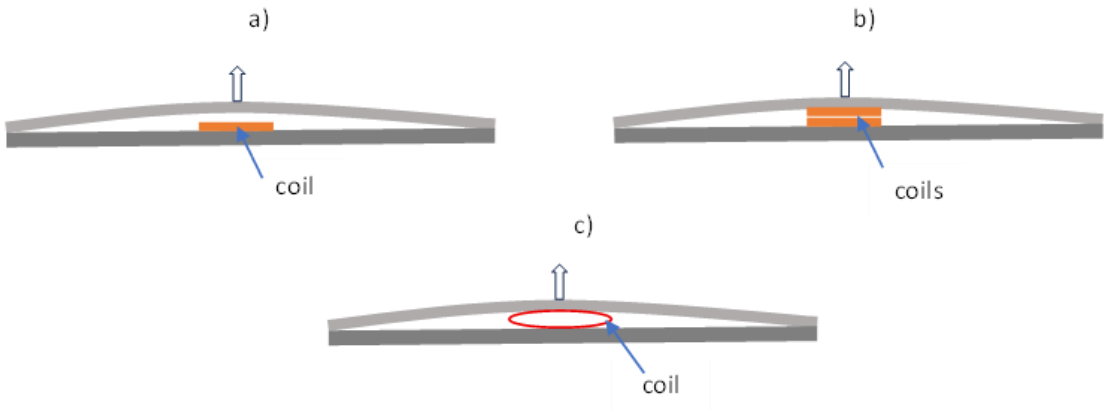

Figure 1. Three options for the EID coil design. a) Single solid coil inducing eddy currents in the aluminum “skin” membrane (Igor Levin’s original design). b)Two solid repulsing each other coils. c) Single flexible double-layer coil wound with either copper ribbons (Cox and Company Co. [14]) or Litz wire (this study).

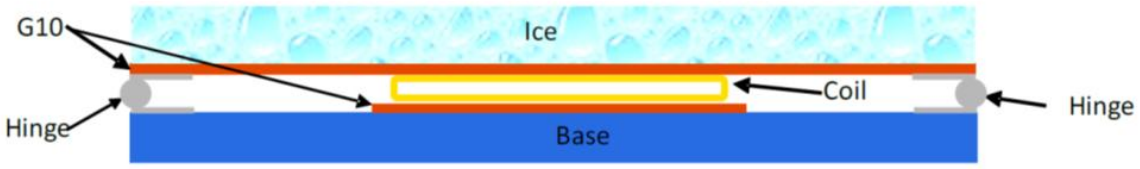

Figure 2. Type 1c EID with simple support (hinges).

Fig. 2 presents simplified schematics of the EIDs used in this study.

III. Theory of EID

The theory of the EID is similar to the theories of other moving electromagnetic coils, such as electric motors, electromagnetic plungers, and actuators. Because the EID theory should combine calculations of electromagnetic fields, electric circuit current and voltage, solid mechanics, and adhesion, the most accurate theoretical method is the use of numerical multi-physics modeling software such as COMSOL Multiphysics or ANSYS. We do not pretend to add new theoretical ideas, but we present below what we have used to design and optimize the EID prototypes.

3.1 Minimization of EID energy requirement

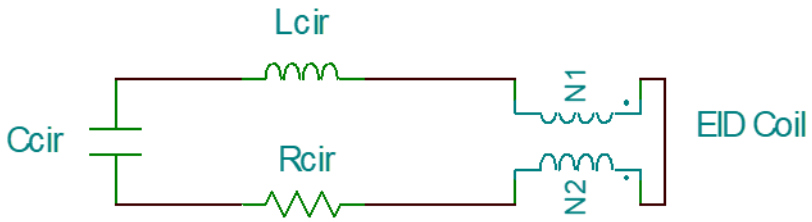

Figure 3. An electrical circuit was used for the theoretical calculations.

Fig. 3 shows the electrical circuit used in our calculations of the electrical parameters. C_{cir} is the energy storage capacitor of the C_C capacitance, L_{cir} is the rest of the circuit inductance (inductance of all lids), R_{cir} is the rest of the circuit resistance (Equivalent Serial Resistance (ESR) of the lids, capacitor, and SCR switch), and EID Coil is the double-sided EID coil of the L_{EID} inductance, with N1 = N2. The initial capacitor voltage was V_0. The total EID inductance is $L_{tot} = L_{EID}+L_{cir}$, and the total EID serial resistance is $R_{tot} = R_{cir} + R_{EID}$, where R_{EID} is the resistance of the EID coil. By applying the Energy Conservation Law (ECL), we can write

$$\frac{C_C(V_0-V(t))^2}{2} = \int_0^t I(t)^2 R_{tot}\, dt + K(t) + U(t) + W_{friction}(t) \quad (1)$$

where $K(t)$ is kinetic energy.

$$K(t) = \frac{m_{tot} v_i(t)^2}{2} \quad (2)$$

where $U(t)$ is the potential energy.

$$U(t) = \frac{\alpha_{plate} \cdot \Delta x_i(t)^2}{2} \quad (3)$$

where *I(t)* is the time-dependent circuit current, m_{tot} is the total moved mass equal to the sum of the ice, half of the coil, and two-thirds of the EID skin, v_i is the time maximum space-average velocity of the moving parts, and $W_{friction}(t)$ is the work done by the frictional forces. The latter may include the work of friction in the hinges, work of airflow friction, and work of ice delamination.

We will use the integral of the square of the circuit current in the future because it defines the total mechanical momentum of the EID. The COMSOL modeling and experimental results presented below show that the first term on the right side of Equation1 account for 95 % to 99 % of the total energy stored in the capacitor. Therefore, to optimize the EID system parameters, we used the following approximation:

$$\int_0^\infty I^2 \, dt \cong \frac{C_C \cdot V^2}{2R_{tot}} \quad (4)$$

The kinetic energy and ice adhesion contributions were considered into account later in the COMSOL Multiphysics simulation. We used COMSOL Multiphysics magnetic field modeling to approximate the magnetic pressure P_M applied to the EID skin by a double-sided coil. The results are presented in Equation 5.

$$P_M(I, n, h, d_{Cu}, t_{ins}) = \frac{f_M(n,h,d_{Cu},t_{ins}) \cdot \mu_0}{2} \cdot \left(\frac{I}{d_{Cu}+2t_{ins}}\right)^2 \quad (5)$$

where *n* is the number of coil turns, *h* is the distance between the centers of the two coil wire layers, d_{Cu} is the equivalent solid copper wire diameter of the Litz wire, and t_{ins} is the apparent thickness of the Litz wire insulation. t_{ins} can be either measured or calculated using a known copper fill factor. The factor $f_M(n, h, d_{Cu}, t_{ins})$ is presented as

$$f_M(n, h, d_{Cu}, t_{ins}) = 2.24 \cdot r(n, , h, d_{Cu}, t_{ins})^4 - 5.15 \cdot r(n, h, d_{Cu}, t_{ins})^3 + 4.64 \cdot r(n, h, d_{Cu}, t_{ins})^2 - 2.4 \cdot r((n, h, d_{Cu}, t_{ins})) + 1.0 \quad (6)$$

where:

$$r(n, h, d_{Cu}, t_{ins}) = \frac{h}{n \cdot (d_{Cu} + 2t_{ins})} \quad (7)$$

Fig. 4 shows the dependence of the magnetic pressure factor on the number of coil turns.

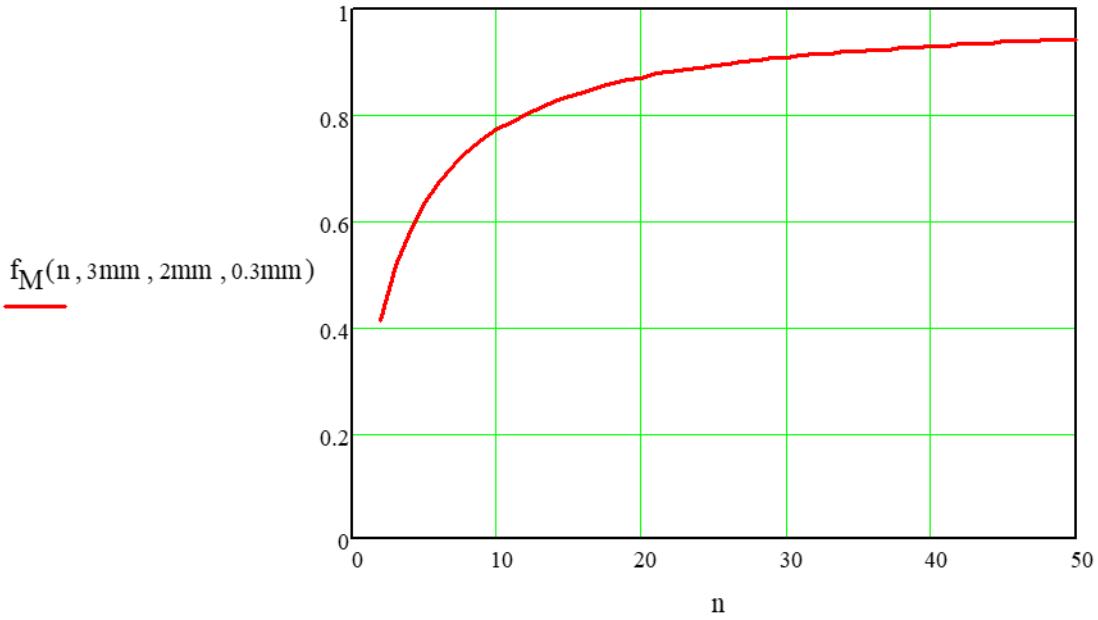

Figure 4. Magnetic pressure factor f_M as a function of number of wire turns, n. h = 3 mm, d_{Cu} =2 mm, t_{ins} = 0.3mm.

The magnetic pressure P_M is equal to the density of the magnetic field energy inside the coil (J/m^3). The inductance of the EID coil is expressed as

$$L_C(A_{EID}, n, h, , d_{Cu}, t_{ins}) = A_{EID} \cdot h \cdot \frac{dP_M(I,n,h,d_{Cu},t_{ins})}{dI} \quad (8)$$

where A_{EID} is the coil area and h is the distance between the centers of the coil layers.

The total momentum of the force applied by the EID coil to the EID skin is presented as

$$M_M(V_0, C_C, A_{EID}, n, h, d_{Cu}, t_{ins}) = A_{EID} \cdot \int_0^{\infty} P_M(I, n, h, d_{Cu}, t_{ins}) dt \quad (9)$$

and it is proportional to the integral of Equation 4. The total momentum in Equation 9 defines the maximum velocity of the ice sheet, EID skin, and upper half of the coil prior to ice delamination:

$$v_{Max}(V_0, C_C, A_{EID}, n, h, d_{Cu}, t_{ins}) = \frac{M_M(V_0, C_C, A_{EID}, n, h, d_{Cu}, t_{ins})}{m_{tot}} \quad (10)$$

where m_{tot} is the "apparent" total mass of the moving parts. At the initial stage of the motion, when the ice sheet and EID skin are bent together, the average moving-part displacement is equal to 2/3 of the maximum skin displacement that occurs at the skin center, as shown in Figs. 1,2.

Because the average displacements, velocities, and accelerations of the moving parts are less than those at the skin center, we can use the reduced mass as follows:

$$m_{tot} \approx \frac{2}{3}(m_{ice} + m_{skin}) + \frac{1}{2}m_{coil} \quad (11)$$

The displacement and velocity vary from their maximum values at the EID center to zero at the hinges.

The total momentum in Equation 9 is a function of seven variables. This makes EID design using a "trial and error approach" impossible. Instead, to minimize the EID energy requirement and/or maximize the total momentum, we used one of the MathCad 15 software optimization functions. Similar optimization functions are available in MATLAB, Mathematica, and Maple software. The results of two optimization examples are presented below.

Example of optimization #1

The input parameters: Carbon-Fiber Composite (CFC) plate with dimensions of 305 mm x 305 mm x 2.2 mm, C_C = 1.5 mF, v_{Max} = 4.5 m/s, t_{ice} = 5 mm, and t_{ins} = 0.3 mm. The three optimization variables were $A_{.EID}$, h, and $d_{Cu.}$ The given limits were $d_{Cu} \leq 2.0$ mm and $A_{.EID} \leq 0.01$ m^2. The calculated optimized parameters were $A_{.EID}$= 0.01 m^2, h = 2.2 mm, and d_{Cu} = 2.0 mm (AWG12). The calculated EID voltage *was* V_0 = 471V, the number of turns was n = 40, the maximum current was 4.46 kA, and the energy density requirement was 1.79 kJ/m^2.

Figs. 5-7 below illustrates the dependence of the EID performance on the capacitor voltage and deicer area.

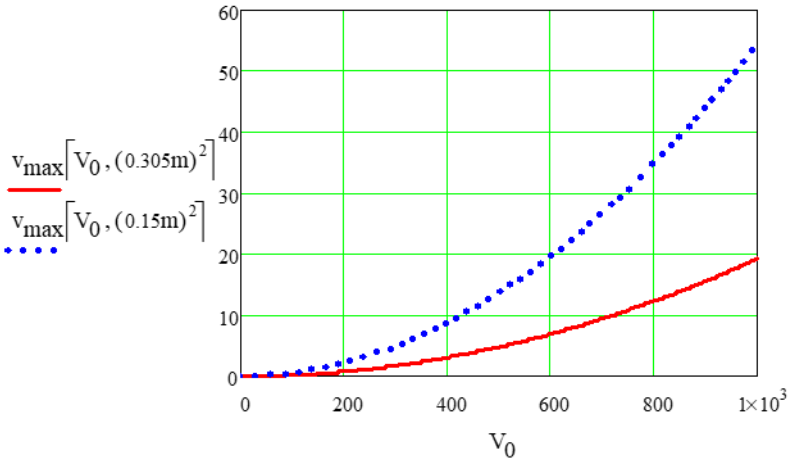

Figure 5. Dependence of the maximum velocity of the moving parts (m/s) on the initial capacitor voltage, V_0. The solid red line is for $A_{PETD} = (305\ mm)^2$, and the blue dotted line is for $A_{PETD} = (150\ mm)^2$.

As shown in Fig. 5, the maximum ice velocity is a parabolic function of voltage.

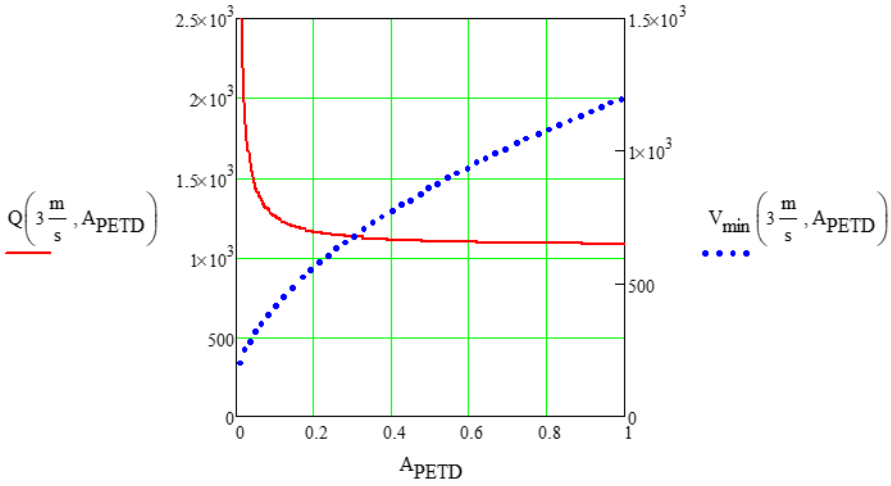

Figure 6. Dependence of the EID density of energy requirement, *Q (J/m2)*, red solid line, and of the initial capacitor voltage, *V* (blue-dot line), on the area of the EID deicer, m^2. The maximum moving-velocity of the parts was 3 m/s.

Fig. 6 shows that the energy density requirement decreases with increasing area of the deicer. The larger the protected area, the less energy per square meter is required.

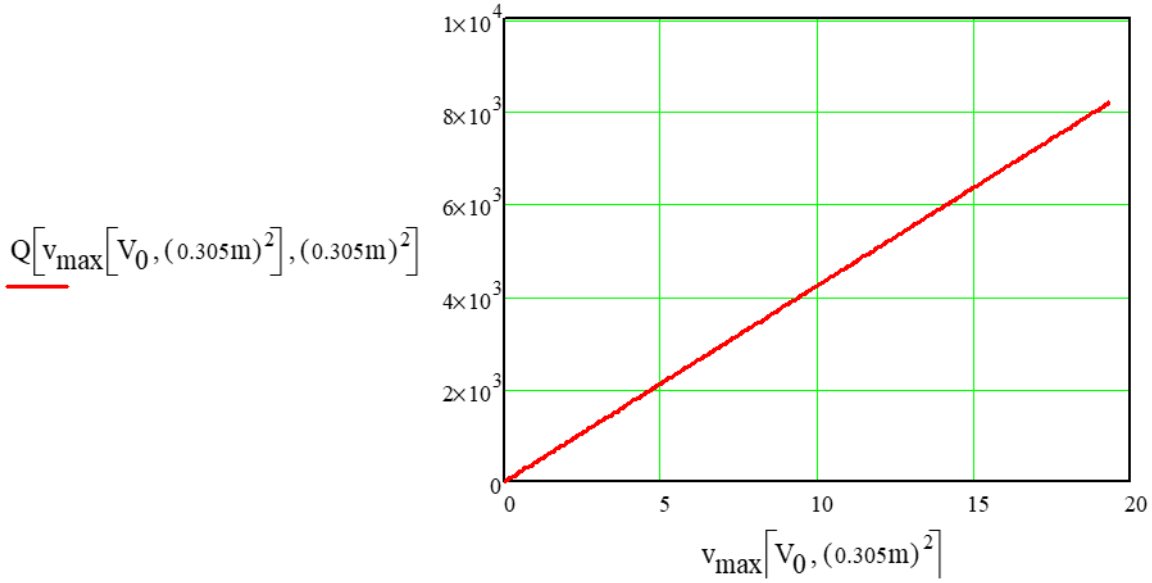

Figure 7. The energy density requirement Q, J/m^2, versus the maximum velocity v, m/s.

Fig. 7 shows that the energy density requirement is a linear function of the maximum ice velocity. This, of course, ignores the low energy density required to brake ice adhesion.

In the example shown above, the damping parameter of the electric circuit ξ was less than one (0.54), thus resulting in an oscillating current. To prevent the current oscillation, we added the requirement of the shortest electric current pulse length with no oscillations (ξ = 1). The result of this modification is presented as an example of optimization #2.

Example of optimization #2

The input parameters were as follows: UHMWPE plate with dimensions of 150 mm x 150 mm x 1.6 mm, C_C = 1.5 mF, v_{Max} = 3.3 m/s, t_{ice} = 5 mm, t_{ins} = 0.3mm. The optimization variables were $A_{.EID}$, h, and $d_{Cu.}$ Given limits: $d_{Cu} \leq$ 2.59 mm and $A_{.EID} \leq$ 25 cm^2. The calculated optimized parameters were $A_{.EID}$ = 25 cm^2, h = 2.5 mm, and d_{Cu} = 1.02 mm (AWG18). The calculated EID voltage was V_0 = 250V, n = 20, maximum current I_{max} = 2.0 kA, energy density requirement Q_{EID} = 2.02 kJ/m^2, and circuit damping parameter ξ = 1.0.

Example of optimization #3, full scale, A_{PETD}= 1 m^2

This is an example of the optimization of a full-scale EID. The input parameters were as follows: CFC plate with dimensions of 1 m x 1 m x 2.2 mm, C_C = 3 mF, v_{Max} = 4.5 m/s, t_{ice} = 5 mm, t_{ins} = 0.3mm. The optimization variables were $A_{.EID}$, h, and $d_{Cu.}$ The limits are $d_{Cu} \leq$ 2.59 mm and $A_{.EID} \leq$ 0.1 m^2. The calculated optimized parameters were $A_{.EID}$ = 625 cm^2, h = 2.5 mm, and d_{Cu} = 1.94 mm (close to that of AWG12). The calculated EID voltage was V_0 =

950V, n = 100, maximum current I_{max} = 2.5 kA, $\int_0^\infty I^2\,dt = 4400\,A^2s$, energy density requirement Q_{EID} = 1.34 kJ/m^2, and circuit damping parameter ξ = 1.39.

The three simple optimizations described above provide a set of parameters for the preliminary design of an EID coil. Now, we must consider four more components of EID physics: ice decohesion energy and the associated force, EID plate bending and vibrations, effect of dynamic coil expansion on the EID current, and time-dependent stress in EID skin and ice. Note that the stress cannot be calculated using the well-known formula for static beam bending.

3.2 COMSOL modeling

We found a significant number of publications devoted to the Final Element Analysis of EID systems. Examples are provided in [10, 14-18]. Unfortunately, neither of these studies provided a detailed description of the simulation sufficient for reproduction. Therefore, we created our own EID simulation using COMSOL-Multiphysics software. The following COMSOL-Multiphysics 5.4 modules were used for the simulation.

1. Solid Mechanics with Adhesion sub-module.
2. Electric circuits of AC/DC module.
3. Magnetic fields.

The simulation included ice adhesion as part of the COMSOL Solid Mechanics Contact option. The Multiphysics simulation also coupled the magnetic fields of the coil with the AC/DC circuit current and coil expansion.

Although we simulated all the EID prototypes presented in the experimental section of the manuscript, we only show the most important results of four simulations.

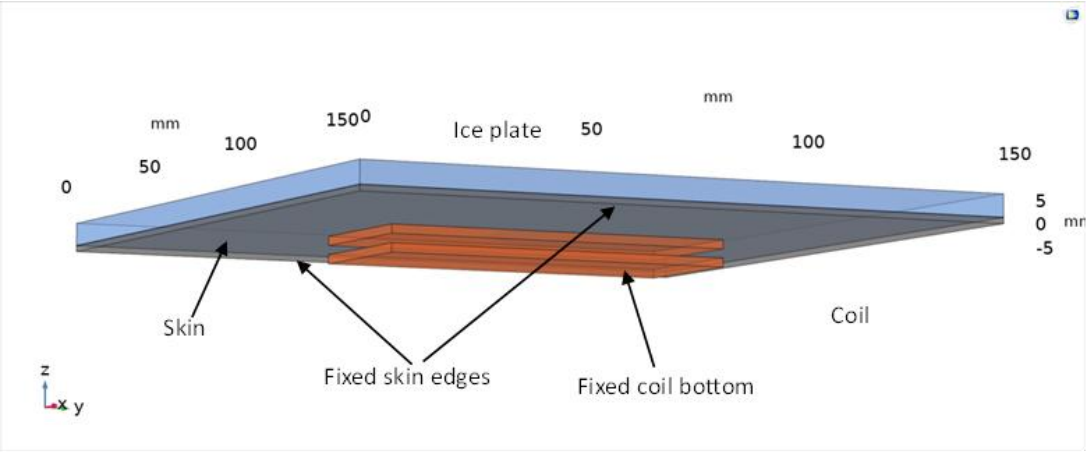

Figure 8. COMSOL-Multiphysics modeling geometry, ice plate.

COMSOL simulation example No.1

Fig. 8 shows the geometry used in this simulation. The following parameters, which closely copy the parameters of Example of Optimization 1, were used:

1. 305 mm × 305 mm × 2.2 mm carbon fiber composite (CFC) plate as the EID skin.
2. 0.1m x 0.1m double-layer EID coil wound with 41 turns of AWG12 Litz wire
3. (d_{Cu} = 2.0 mm). The copper volumetric fill was 60%.
4. 1.5 mF film capacitor with an initial voltage of V_0 =500V. The peak current *was* I_{max} = 4.6 kA.
5. The air temperature T_{air} was -10°C. Time step 1 μs.
6. The normal and shear ice adhesion strengths were 50 kPa [23].
7. The energy density *was* Q_{EID} = 2.02 kJ/m^2. The maximum ice velocity *was* 5.2 m/s.
8. The maximum volume-average CFC von Mises stress was 130 MPa.
9. The maximum volume-average ice von Mises stress was 13 MPa.

Fig. 9–11 show the simulation results. Fig. 9 shows the coil current as a function of the time. The maximum current was 4.6 kA, which was close to the optimization prediction of 4.46 kA. The difference between the currents of the optimization and simulation was not significant.

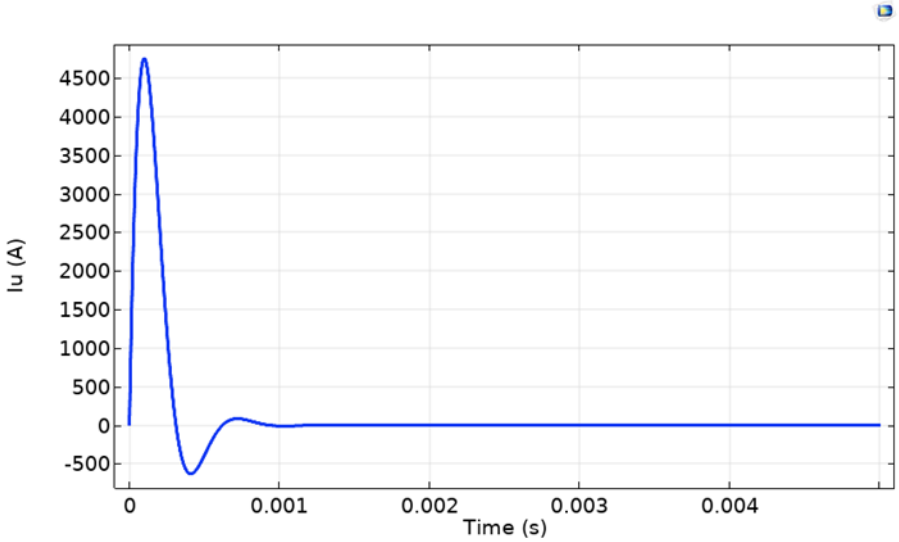

Figure 9. Coil current, A, versus time, s.

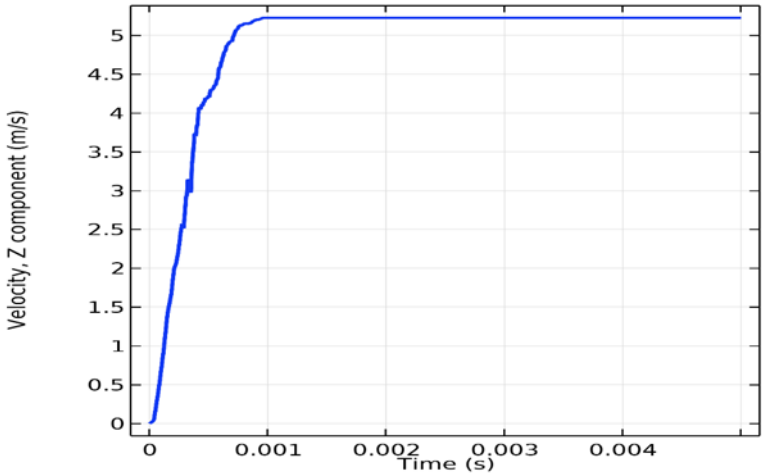

Figure 10. The ice sheet volume-average velocity (m/s) versus time (s) smoothed the ice plate vibration.

Fig. 10 shows the ice velocity versus time. The ice plate was separated from the skin at 1 ms.. The maximum velocity of 5.2 m/s is close to the 4.5 m/s predicted in the Example of optimization #1.

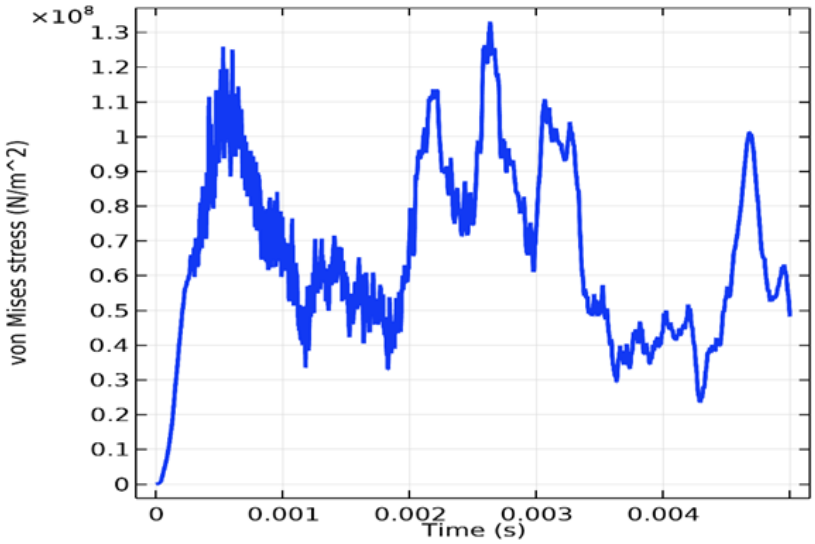

Figure 11. Volume-average von Mises stress in the CFC, MPa, versus time, s.

Fig. 11 shows the volume-average von Mises stress of the CFC plate. Notice that the maximum stress is approximately one order of magnitude less than the known ultimate strength of the CFC composites (1–1.6 GPa).

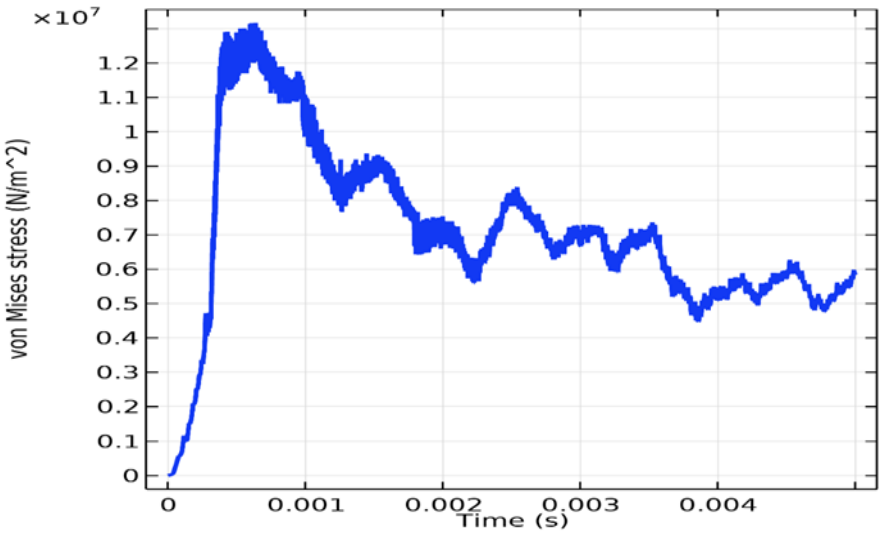

Figure 12. Volume-average von Mises stress in the ice plate, MPa, versus time, s.

Fig. 12 presents the volume-average von Mises stress of the ice plate. Notice that the maximum stress is approximately one order of magnitude higher than the known ultimate strength of solid polycrystalline ice (0.5–1.5 MPa range). This means that the ice plate should be broken into pieces. This is what we and other researchers have observed. We failed to add the Fracture Mechanics module to the simulation because even without it, a single simulation required approximately 24h. Such an addition to the simulation compromises the convergence of the calculations. To determine how cracked ice is shed, we placed multiple small 1 cm3 cubes on the EID skin, as described in the following section. These cubes were used in our experimental tests. Averaging smooths the high-frequency noise in the data.

COMSOL simulation example No.2

Fig. 13 shows the geometry used in this simulation.

1. A 152 mm × 152 mm × 1.27 mm 2024 aluminum plate was coated with a 0.075 mm-thick UHMWPE film as the EID skin. The ice adhesion strength = 49 kPa [5].

81 mm x 34 mm double-layer EID coil wound with 20 turns of AWG18 Litz wire (dCu = 1.02 mm). (The copper volumetric fill was 60%.

1.5 mF film capacitor with an initial voltage of V0 =250V. The peak current was Imax = 1.94 kA.

The circuit was fully damped with a damping factor of 1.0.

The air temperature Tair was -10°C. Time step 1 μs.

The energy density was QEID = 2.02 kJ/m2. The central ice cube velocity was 7.4 m/s.

The maximum volume-average aluminum von Mises stress was 95 MPa.

The maximum volume-average ice von Mises stress was 0.75 MPa.

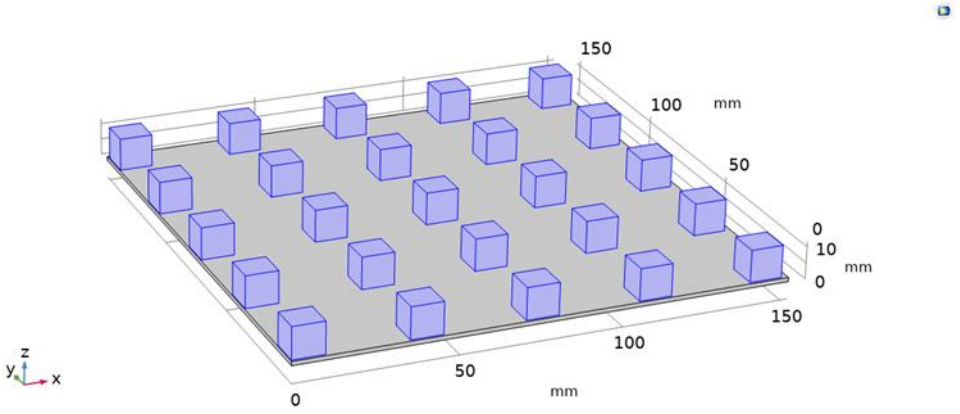

Figure 13. COMSOL-Multiphysics modeling geometry, ice cubes.

Figs. 14-17 present the simulation results. Fig. 14 presents the von Mises stress in the aluminum and ice cubes and the part displacement at 0.003s. The stress in the Al plate is non-uniform because of the plate vibrations. The ice cube displacement was maximum at the center of the plate and minimum near the fixed plate edges (x =0 mm and x = 152 mm).

Fig. 12 shows the coil current as a function of time. The maximum current was 1.94 kA.

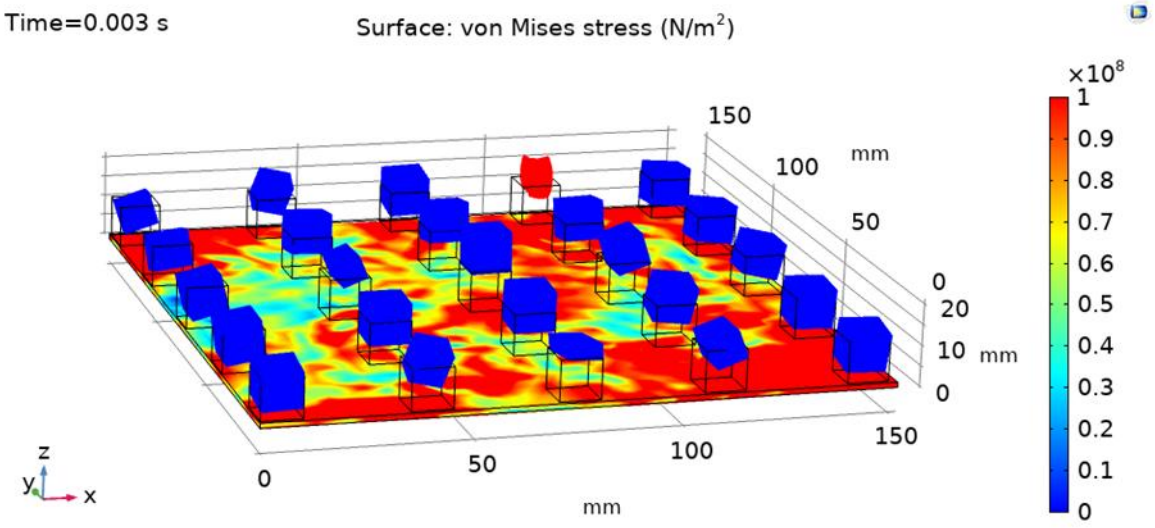

Figure 14. Von Mises stress and displacements at 0.003 s.

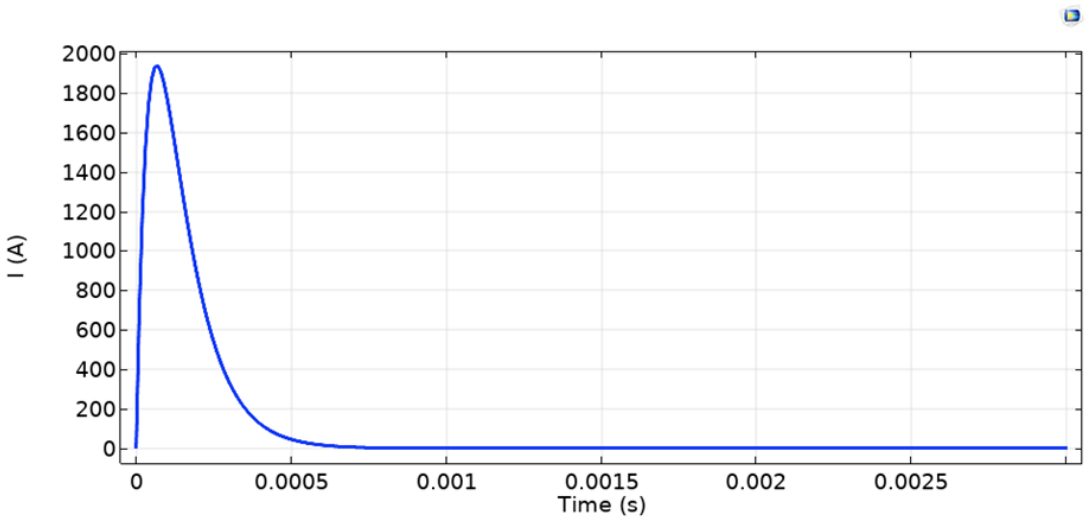

Figure 15. Coil current, A, as a function of time, s

Fig. 16 presents the velocity of the central ice cube, m/s, as a function of time, s The maximum ice cube velocity was higher than that predicted by the optimization for ice thickness equal to 5 mm because the average ice thickness on the plate with cubes was only 1.1 mm.

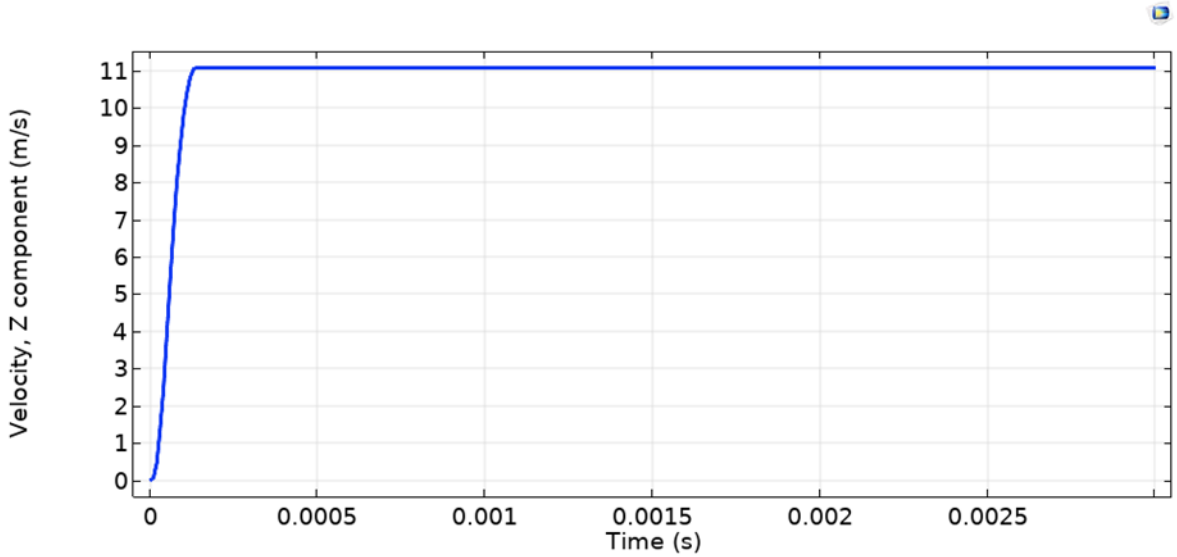

Figure 16. Velocity of the central ice cube, m/s, as a function of time, s. The ice was separated from the aluminum plate at approximately 0.2 ms.

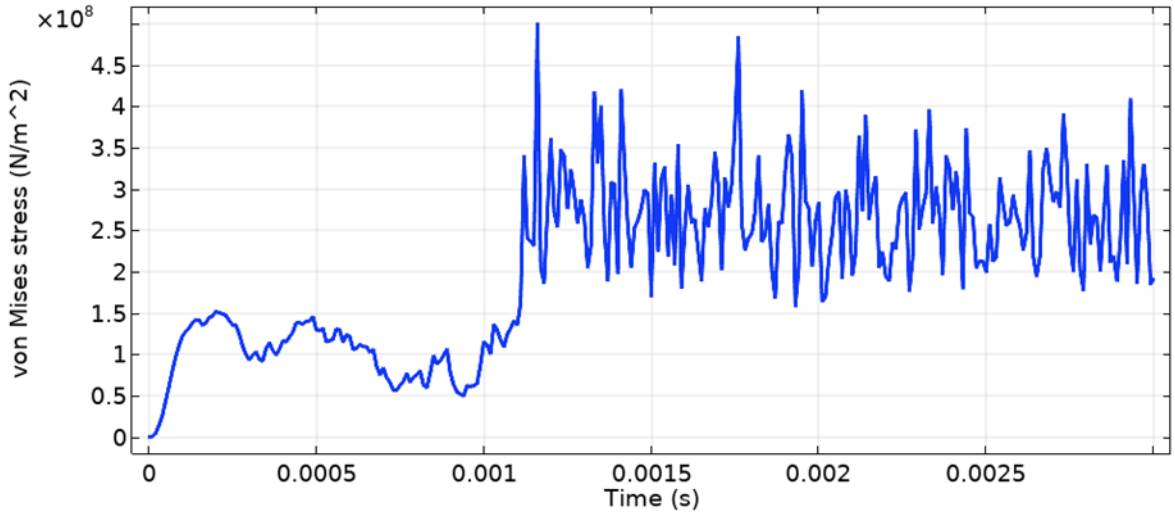

Figure 17. Aluminum maximum von Mises stress, Pa, versus time, s.

Fig. 17 shows the maximum von Mises stress in the aluminum plate as a function of time. Note that the maximum stress is lower than the yield stress of the 2024 aluminum alloy (690 MPa).

Fig. 18 presents the volume-average von Mises stress in the central ice cube as a function of time, t. The maximum stress of 0.75 MPa is comparable to the maximum strength of polycrystalline ice.

We modeled the thin UHMWPE film as a "Thin Elastic Layer" option of COMSOL Multiphysics Solid Mechanics. The addition of the film did not change the results.

The maximum stress in the UHMWPE film can be estimated as the maximum stress in the aluminum plate multiplied by the ratio of the elastic moduli of the two materials. Such an estimate assumes the continuity of the tangential strain in the film and aluminum plate.

$$\sigma_{UHMWPE} = \frac{690MPa}{72.4GPa} \cdot 95MPa = 0.9MPa \qquad (11)$$

This is much lower than the ultimate strength of UHMWPE of 43.5 MPa.

A PTFE thin film, which we also used in our experiments, has an even lower adhesion strength to ice (39 kPa) and comparable mechanical properties to UHMWPE.

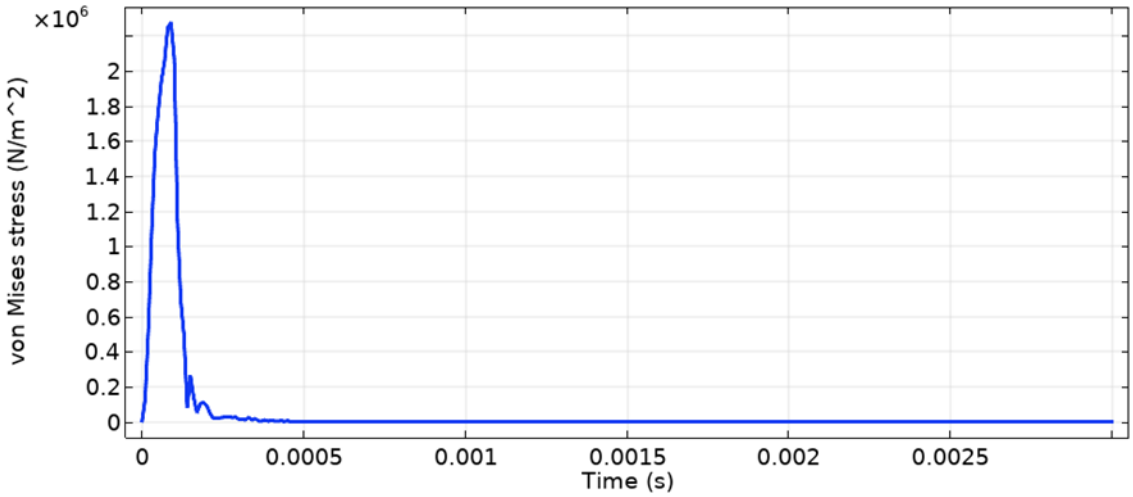

Figure 18. Volume-average von Mises stress in the central ice cube, Pa, vs. time, s.

COMSOL simulation example No.3 and No.4

For these simulations, we used an Aluminum 2024-T4 plate with a diameter of 17.2 cm and a thickness of 1.59 mm. The 1a EID configuration is the most commonly used and is shown in Fig. 1a. To facilitate the comparison of this option with the others, we used the same total deicer area APETD and coil area AEID as in MathCad Option No. 2 and COMSOL Option No. 2. Because the coils of option 1a were circular, we used a circular Al plate. The plate was coated with a thin 0.075 mm UHMWPE film. The axisymmetric geometry of the deicer required a much shorter calculation time and improved convergence.

Below, we summarize the results of this simulation.

1. D = 17.2 cm, tAl= 1.59 mm. 2024 aluminum plate coated with a 0.075 mm thick UHMWPE film. The ice adhesion strength = 49 kPa [5].

2. Single-layer EID coil of R1=2 cm and R2=3.5 cm was wound with 9 turns (18 of No.4) of AWG18 Litz wire (dCu = 1.0 mm) and had copper volumetric fill coefficient of = 0.6.

The ice plate thickness was 5 mm. 1.5 mF film capacitor with an initial voltage of V0 =250V. The peak current Imax was 2.945 kA.

The air temperature Tair was -10°C. Time step 1 μs.

The energy density was QEID = 2.02 kJ/m2. The maximum ice sheet velocity was 0.9 m/s and 1.27 (No. 4).

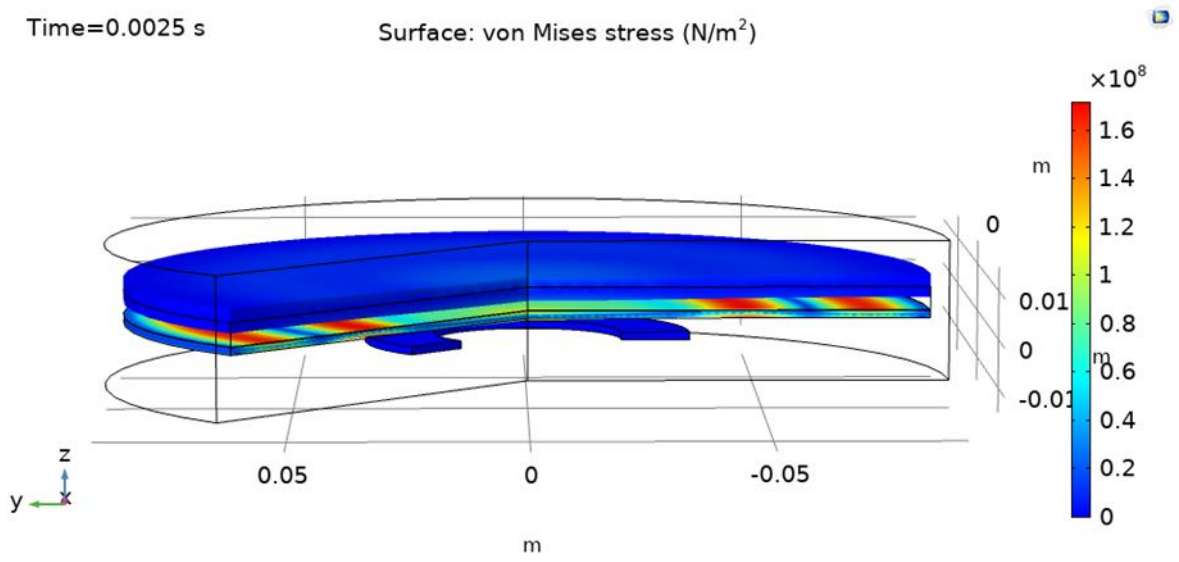

Figure 19. Geometry of COMSOL Option No. 3 simulation and maximum magnetic flux density *B*, T, at 69 μs.

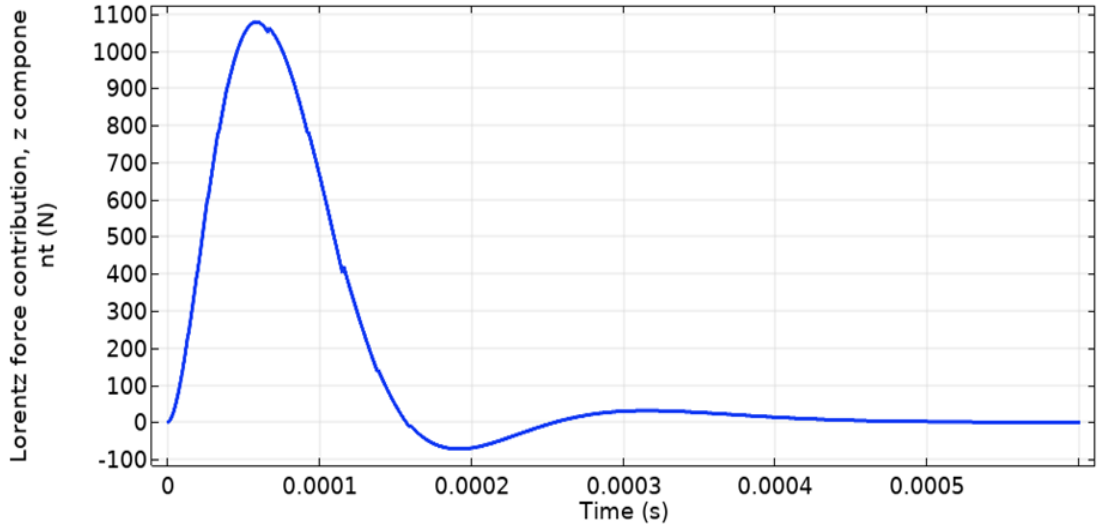

Figure 20. Lorentz force on the aluminum plate, N, versus time, s COMSOL option no. 3.

Fig. 20 presents the electromagnetic (Lorentz) applied to the aluminum plate as a function of the time. The total momentum of the force was 0.09 N·s (0.18 of Option 4). For comparison, the same area double-sided coil of COMSOL Option No. 2 provided a total force momentum of 0.212 N·s, which was 2.3 times higher. Therefore, we concluded that the 1c coil configuration is better than that of 1a. This conclusion was also supported by the lower ice velocity of COMSOL Option No. 3.

Table 1. Comparison of COMSOL simulation with MathCad optimization results.

Software	v_{ice} m/s	Q_{EID} kJ/m^2	d_{Cu} mm	R_{tot} ohm	L_{tot} μH	ζ	A_{EID} cm^2	σ_{skin} MPa	σ_{ice} MPa
MathCad Option 1	5.1	2.02	2	0.06	4.6	0.54	100	NA	NA
Math Cad Option 2	3.3	2.02	1.02	0.095	5	1	25	NA	NA
MathCad Option 3	4.5	1.34	1.94	0.307	37	1.39	625	NA	NA
COMSOL Option 1	5.2	2.02	2	0.06	4.6	0.54	100	130	13
COMSOL Option 2	11	2.02	1	0.095	5.02	1	25	500	2.3
COMSOL Option 3	0.9	2.02	1	0.01	NA	NA	25	170	12
COMSOL Option 4	1.27	2.02	1	0.01	NA	NA	25	280	18

3.3 Theoretical Summary

Although we have only provided detailed results for six optimizations/simulations, the total number of them was well over 100. Most of our theoretical findings are summarized as follows.

1. A simple and efficient design algorithm was developed. The algorithm is based on the proportionality of the total mechanical momentum of the moving EID parts to the ratio of the energy stored in a capacitor to the total circuit resistance.
2. The use of MathCad optimization software enabled a significant reduction in the energy requirements of the EID.
3. The results of the COMSOL simulation supported the MathCad optimization predictions. The COMSOL simulation provided important information on the stress developed in EID systems built using various materials.
4. The EID with a Carbon Fiber Composite skin appeared to be the best.
5. The second-best EID performance was aluminum-alloy EID coated with low ice adhesion films of UHMWPE and PTFE.
6. EIDs with a bare aluminum-alloy skin were the worst performers.
7. Single-layer EID coils (Fig. 1a) were the worst performers compared to coils 1b and 1c.
8. The maximum stress in the designed EID skin was below the yield stress of the skin material.
9. The stress applied to the ice sheets should crack the ice.
10. In addition to low-frequency bending waves, the EID generates high-frequency sonic waves.
11. Because of the very short pulses of the EID current, EID coils should be wound with either Litz wires or thin copper foils (skin-effect phenomenon).
12. Litz-wire coils are superior to copper-foil ribbons.

IV Materials selection

1. Carbon Fiber Composite (CFC) with a twill weave. The ice adhesion strength of carbon fiber composite materials is generally considered to be relatively low. For instance, a study demonstrated that after undergoing 30 cycles of icing and de-icing, the surface of the composite retained an ice adhesion strength of less than 50 kPa [23]. Moreover, the CFC surface exhibited impressive hydrophobic characteristics, as indicated by a water contact angle greater than 150°. This high contact angle not only signifies excellent water-repelling properties but also plays a critical role in reducing ice adhesion, making carbon-fiber composites an attractive choice. The weave type of CFC plays a very important role. The weaves that provide the largest contact area between the carbon fibers and ice demonstrate the highest water contact angle. Twill weave is the best option because it provides close to 100% area filled with carbon fibers. Carbon fibers are UV resistant, whereas most binding epoxies are not. We tested two EIDs made of CFC.

2. Ultra-High Molecular Weight Polyethylene (UHMWPE) is one of the best low ice adhesion and low interfacial toughness materials [5].This material is used in other applications, such as high-performance ropes, slings, and netting, because of its high strength-to-weight ratio, low friction, and excellent chemical resistance. It is not UV-resistant, but it can become UV resistant. UHMWPE is widely available as sheets and single-sided adhesive films. We tested one EID made of a solid UHMWPE sheet, one EID made of an Aluminum 6061sheet coated with a UHMWPE film, and one EID made of an FR4 composite sheet coated with a UHMWPE film.

3. PTFE (Teflon) is another low-ice adhesion/low interfacial toughness material [5]. Teflon has excellent UV and chemical resistance and is widely available as sheets and single-sided adhesive films. We tested one EID made of an Aluminum 6061sheet coated with a Teflon adhesive film.

4. Several other materials, such as Poly Propylene (PP), glass-fiber composite (G10), and PETG, have been tested because they combine good mechanical strength with modest adhesion to ice strength.

V. ELECTRONICS

Fig. 21. Presents a simplified schematic diagram of the electronics used to test the EIDs. The optocoupler (MOC223) isolated the low-voltage trigger circuit (left) from the high-voltage ICD circuit (right). The two diodes protect the capacitor and semiconductor-controlled rectifier (SCR) switch from reverse voltage peaks. The peak capacitor discharge currents during testing

varied from 200 to 3 kA. One BT158W SCR can withstand a 3 kA 1-ms current pulse with an I^2t rating of 6,000 A^2s. For some prototypes, we connected up to four BT158W SCRs in parallel. Because of the low resistance of many tested ICDs, most connections were soldered, and 12 and 14 AWG wires were used as leads to minimize the total resistance in the high-current circuit. The capacitor-charger module delivered an output power of 60 W with a maximum output voltage of 900 V. All the capacitors used in this study were film capacitors, featuring a very low estimated series resistance (ESR) of approximately 1 mΩ. The circuit shown in Fig. 21 was used for several hundred pulses throughoutt the testing period. The EID coils were wound with high-frequency conductive Litz wires.

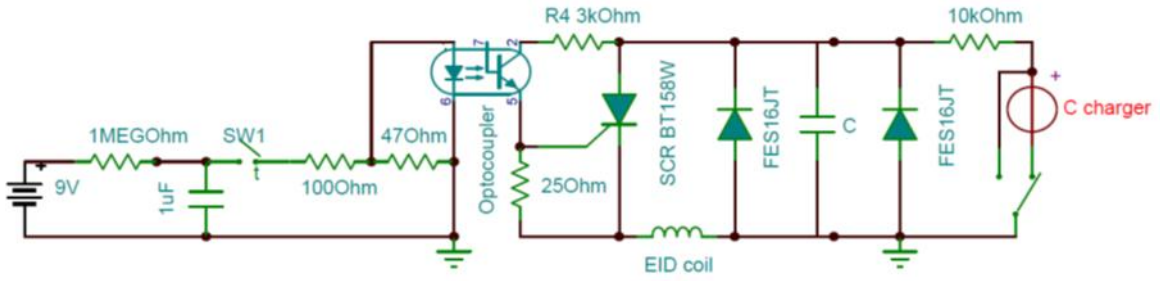

Figure 21. Simplified schematic diagram of the electronics used to test the EIDs.

VI. OTHER EQUIPMENT

Testing of all EID prototypes was performed inside a freezer chamber at temperatures ranging from 0 °C to -20 °C. The temperature was measured using a thin-film thermocouple attached to the back of the prototypes. The circuit current was recorded using a digital oscilloscope.

In most of the tests, we used 20–40 1 cm × 1 cm × 1 cm ice cubes grown in tap water in a plastic ice tray. The ice cubes were then attached to drops of water on the cold EID skin and allowed to refreeze. Most tests were recorded on video. The approximate velocities of the ice cubes were measured by playing the video clips frame-by-frame using Microsoft Clipchamp software. Fig. 22 presents a UHMWPE plate of 152 mm × 152 mm × 1.6 mm with 20 1 cm^3ice cubes.

Fig. 20. presents the UHMWPE plate and flying ice cubes 40 ms after an EID pulse was applied. Few central ice cubes already left 20-cm visual area, which means that the cubes velocity was over 20 cm/0.04 s = 5 m/s. The velocities of the peripheral ice cubes were

approximately 1 m/s. The more accurate method of the velocity was measuring the distance over which the ice cubes flew from 1.25 m height above the floor to the floor carpet. However, the maximum velocity that could be measured using the second method was limited by the distance to the opposite wall of the lab (10 m/s).

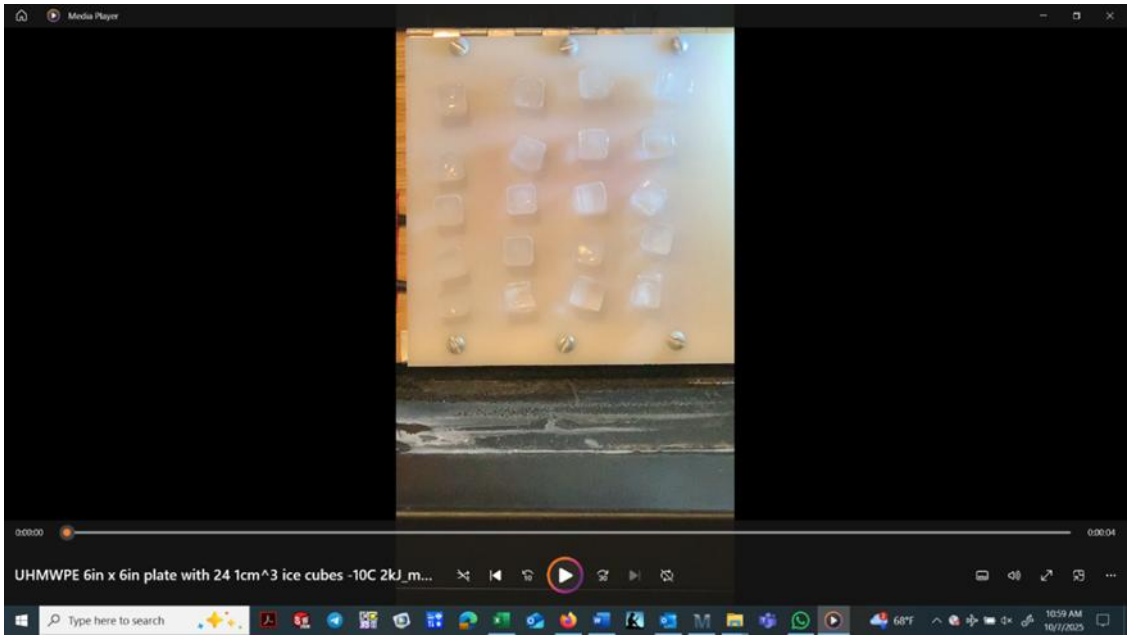

Figure 22. UHMWPE 152 mm × 152 mm × 1.6 mm plate with 20 1 cm3 ice cubes before EID pulse application.

Figure 23. UHMWPE 152 mm × 152 mm × 1.6 mm plate with 20 1 cm3ice cubes 40 ms after an EID pulse was applied.

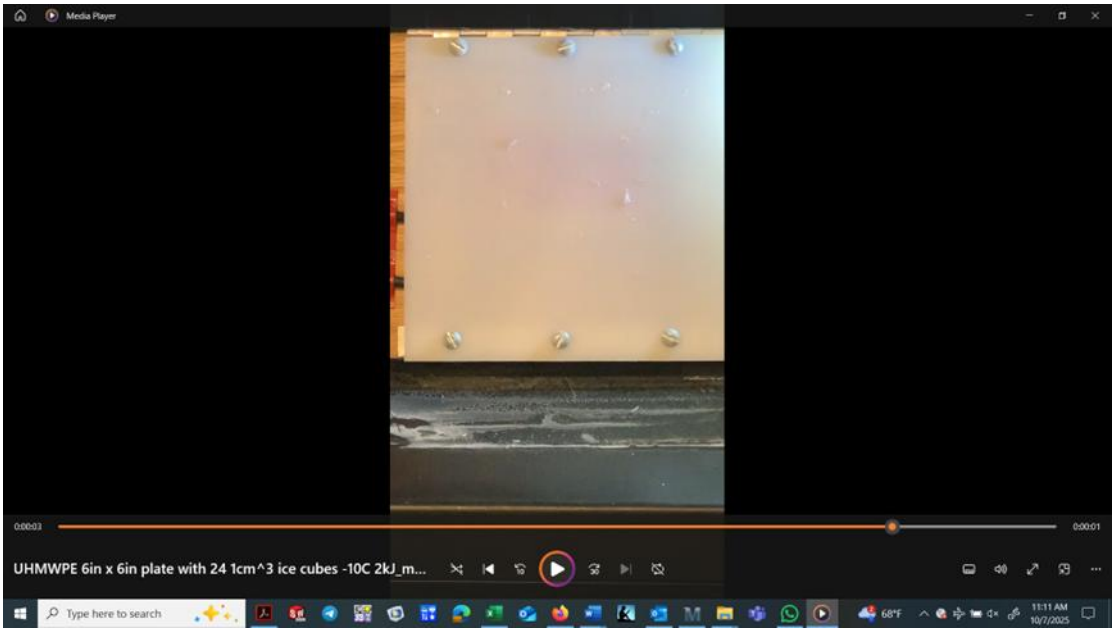

Figure 24. UHMWPE 152 mm × 152 mm × 1.6 mm plate with 20 1 cm3ice cubes. 2 min after the EID pulse was applied.

The ice shedding by the EID was impressive, and the difference between the EIDs built using various materials was mainly the difference in the amount of ice remaining on the surface. A good example of cleaning is shown in Fig.24.

The test results are summarized in Table 2. Each prototype was tested several times. In all tests, a 1.5 mF film capacitor with a maximum voltage of 1.1 kV was used. In most of the tests, the coil presented in COMSOL Option No. 2 was used.

Experimental results

Because the energy requirement, Q, is proportional to the maximum ice velocity, v (Fig.7), we included the calculated energy requirement needed to shed ice at 5 m/s (column 6 of Table 2). This allows for a better comparison of the performance of various materials.

As shown in Table 2, the CFC plates, polymer plates (PETG and UHMWPE), and polymer coating films of PTFE and UHMWPE provided the best ice cleaning. EID made of these materials had the lowest energy density requirement of less than or equal to 2 kJ/m^2. The worst cleaning performance was observed for the 2024 aluminum and glass-fiber composite (G10/FR4) plates. 2024 Aluminum and glass-fiber composite plates require a higher energy density than other materials.

Table 2. Summary of the experimental results. C = 1.5 mF

Skin Material	**Size,** mm	**T_i,** °C	**V,** V	**Q** kJ/m^2	**Q(5m/s)** kJ/m^2	**v_{max},** m/s	**Cleaned area %**
Aluminum	140x110x1.27	-21	400	7.8	NA	0	None
Aluminum	152x152x1.27	-10	387	4.8	9.6	2.5	80%
Aluminum	152x152x1.27	-10	250	2.0	2.5	4	60%
G10/FR4	152x152x1.27	-10	360	4.2	10.5	2	95%
UHMWPE film on G10	152x152x1.27	-10	250	2.0	1.5	6.7	>99%
UHMWPE film on Al	152x152x1.27	-10	250	2.0	2.0	5,	>99%
UHMWPE plate	152x152x1.6	-10	250	2.0	2.0	5	>99%
PTFE film on Al plate	152x152x1.6	-10	250	2.0	< 2.0	>5	>99%
PETG plate	152x152x1.27	-10	200	1.3	1.6	4	>99%
Polypropylene Ice tray	480cm^2	-13	250	1.0	5.0	1.0	>99%
CFC plate	152x152x0.78	-10	250	2.0	**2.0**	5	>99%

VII. Full-Scale Feasibility

Our experimental and theoretical results predict that scaling up a properly designed EID should not be a problem. Let us illustrate this with a design based on MathCad Optimization No.3. Assume that we want to deice a very large building with a total deiced area of 10,000 m^2. We will use 10,000 EID panels 1 m^2 each. All panels were connected in parallel. A single 3 mF × 1100 VDC EPCOS-TDK film capacitor (B25690G1308K103) was used. One capacitor charger of 1.5 kW charges the capacitor to 1 kV in 1 s. The capacitor had an ESR of 0.001 Ω and a weight of 5.7 kg. A single pulse of the capacitor dissipated 4.4 J of thermal energy inside the capacitor. This thermal energy would heat the capacitor by 7.7 °C after 10,000 pulses. Thus, a single capacitor for the entire building would suffice. The energy stored in the capacitor per pulse is 1.5 kJ. Each EID panel has its own BT158W SCR switch. However, SCR switches are

triggered one by one by a square matrix of switches in the same way that a panel of 10000 LCDs is controlled.

CFC- or PTFE-coated aluminum alloy or glass fiber panels can be used as EID skin material. Another option is to use aluminum sheets coated with non-stick PTFE. They are commonly used as baking sheets. Whole-building deicing can be accomplished in less than 3 h. However, the deicing cycle can be shortened by using several capacitors and chargers.

VIII. CONCLUSION

Combining the EID optimization theory with low interfacial toughness materials provided perfect cleaning of ice and the lowest energy density requirement. COMSOL Multiphysics simulation was important in preventing the high mechanical stress caused by EID pulses. The result of this combination was an energy requirement 50 times less than that of the pulse electrothermal deicer and 500 times less than that of traditional thermal de-icing. Simple and accurate algorithms for EID design and design optimization played an important role in the success of this study. The improved EID technology can be applied to the deicing of buildings, bridges, airplanes, evaporators of refrigerators, harvesting of ice in residential, commercial, and industrial icemakers, and in deicing communication equipment such as antennas and radars. In summary, this document presents a compelling case for a paradigm shift in deicing technology. By systematically addressing the core weaknesses of EID systems through materials science and optimized engineering design, this study demonstratess a practical, highly efficient, and reliable solution with significant potential economic and environmental benefits for a wide range of industries.

IX. ACKNOWLEDGEMENTS

None.

IX. REFERENCES

[1] I Levin, Device for deicing surfaces of thin-walled structures, US Patent No. 3,549,964, 1968.

[2] I Levin, ELECTRIC SYSTEM OF A DEVICE FOR DEICING THE SURFACE OF THIN-WALLED STRUCTURES, US Patent No. 3672,610, 1972.

[3] V Petrenko, SYSTEMS AND METHODS FOR MODIFYING AN ICE-TO-OBJECT INTERFACE, US Patent No. 6,870,139, 2005.

[4] V Petrenko et al., Pulse electrothermal de-icer (PETD), Cold Reg. Sci. Technol. 65(1), 2011,70-78.

[5] K Golovin, A. A. Shcherbina, A. V. Shcherbina, and V. A. Sh Science, 364, 2019, 371-375.

[6] R. Goldschmidt, Electro-impulse de-icing system for aircraft, British Patent No. 505,433; May 5, 1939.

[7] G Zumwalt, R. Schrag, W. Bernhart, and R. Friedberg, Electro-Impulse De-Icing Testing Analysis and Design, NASA Contractor Report 4175**, 1988.**

[8] G. W. Zumwalt, R. L. Schrag, W. D. Bernhart, and R. A. Friedberg, Electro-Impulse De-Icing Testing Analysis and Design. NASA Contractor Report 4175**. 1988.**

[9] De-icing for the Il-114, https://www.flightglobal.com/de-icing-for-the-il-114/577.article.

[10] W Bernhart, G. Zumwalt, Electro-impulse deicing-Structural dynamic studies, icing tunnel tests and applications, 22nd Aerospace Sciences Meeting, 1984•arc.aiaa.org.

[11] R Henderson and R. Schrag, Theoretical Analysis of the Electrical Aspects of the Basic Electro-Impulse Problem in Aircraft De-Icing Applications, NASA Contractor Report 180845 (1987).

[12] P Zieve, Self-contained apparatus for deicing aircraft surfaces using magnetic pulse energy, U.S. Patent No. 4,895,322, 1992.

[13] R Scavuzzo et al., Finite element studies of the electro impulse de-icing system Journal of Aircraft, 27(9),1990.

[14] COX and Company EID webpage. https://www.coxandco.com/low_power_ips.html.

[15] A Kodet. Electro-Impulsive Dicing, 1988, IEEE, 88TH0220-4.

[16] J Gerardy and R. Ingram., ELECTRO-MAGNETIC EXPULSION DE-ICING SYSTEM, J Ingram, 2000, US Patent No. 6,102,333.

[17] X Jiang and Y. Wang, Studies on the Electro-Impulse De-Icing System of Aircraft, Aerospace, 6(6), 2019, 67.

[18] Q Li, T. Bai and C. Zhu, De-icing excitation simulation and structural dynamic analysis of the electro-impulse de-icing system, Appl. Mech. Mater., 66–68, 2011, 390–395.

[19] G Li, J. He, Y., and Lin, Y., Analysis on structural dynamics of simplified EIDI system, Beijing Univ. Aeronaut., 5, 2015, 1–6.

[20] Q Li, C. Zhu, and T. Bai, Simplification of de-icing excitation and influential factors of the electro-impulse de-icing system, J. Aviat., 25,2012, 1384–1393.

[21] E Moehle, M. Haupt, and P. Horst, Coupled Magnetic and Structural Numerical Simulation and Experimental Validation of the Electro-Impulse De-Icing, in Proceedings of the 54th AIAA/ASME/ASCE/AHS/ASC Structures, Structural Dynamics, and Materials Conference, Boston, MA, USA, April 2013, pp.8–11.

[22] M Endres, Experimental study of two electro-mechanical de-icing systems applied on a wing section tested in an icing wind tunnel, J. CEAS Aeronautic, 8, 2017, 429–439.

[23] Y. Xu et al., Study on anti-icing performance of carbon fiber composite superhydrophobic surface, Materialstoday Chemistry, 29, 2023, 1-13.

Citation: Victor Petrenko. (2025). Development of Ultra-Low Power Deicer for Civil Engineering Applications. Journal of Civil Engineering and Technology (JCIET), 11(2), 1-28.

Abstract Link: https://iaeme.com/Home/article_id/JCIET_11_02_001

Article Link:
https://iaeme.com/MasterAdmin/Journal_uploads/JCIET/VOLUME_11_ISSUE_2/JCIET_11_02_001.pdf

✉ **editor@iaeme.com**